Supplementary Material for

„Disrupted intrinsic networks link amyloid plaques and impaired cognition in prodromal Alzheimer's disease"

Supplementary methods and results:

Behavioural task: design and results.

Structural MRI: data acquisition and voxel based morphometry (VBM).

PIB-PET analysis.

Supplementary Figures:

Supplementary Tables:

Behavioral task: design and results.

Design. The task consisted of 4 conditions that orthogonally manipulated motor difficulty and visual difficulty (two difficulty levels each). In the two easiest conditions, visual task difficulty was low: participants were simply required to make a speeded button press response (index or middle finger) to the onset of a scrambled scene (i.e., a real-world scene scrambled by dividing each scene into 40x40 pixels and randomly rearranging the pixels; for sample images please refer to Figure S2). Low motor difficulty demanded responses of only one hand throughout a block of six trials (indicated by a hand symbol presented on one side next to scrambled scenes during a block of trials), while high motor difficulty could require responses from either hand within a block (indicated by randomly changing hand symbols right or left next to scrambled scenes). The more difficult visual conditions additionally required the speeded categorization of a centrally presented stimulus (i.e., a grayscale real-world scene, see Fig. S2) as a city street or country road by index (for street) or middle (for road) finger button press. In the easier visual task condition, responses were made with the same hand throughout a block, while the more difficult blocks could require responses with either hand within a block (as above). This overall design resulted in a total of four difficulty levels (level 1: unimanual motor only, level 2: bimanual motor only, level 3: unimanual motor and visual, level 4: bimanual motor and visual). These conditions should require top-down attention and response execution (level 1), attention, response selection, and response execution (level 2), attention, scene categorization, and response selection and execution (level 3), and finally attention, categorization, two levels of response selection (cued hand and correct finger), and response execution (level 4). Accordingly, processing of the different task conditions should recruit networks relating to the control of top-down attention, scene

categorization, and response selection (i.e., ATN, DMN, motor networks) to different degrees. Due to previous findings of disrupted FC in early AD, we were primarily interested in ATNs and the DMN.

There were six blocks for each of the four task conditions such that there were a total of 24 blocks. Each block started with a brief instruction screen (4.8 s) indicating the visual- and motor-task requirements of the upcoming block, followed by six trials of that condition. Within each block, each trial started with the onset of the visual stimulus (i.e., gray scale picture with or without hand symbol beside) shown for 6 s, followed by a 200 ms inter-trial interval. Between blocks, a fixation cross was presented for 200 ms. The sequence of 24 blocks was pseudorandomized and counterbalanced across participants. Outcome measures were accuracy (ACCR, i.e. the rate of correct button responses) and reaction time (RT). All participants were successfully trained for the task by a standardized procedure within two days before scanning. Our design allowed us to independently test behavioral impairments in the pAD group as a function of varying motor or visual demands. To this end, we performed a three-way mixed-effects analysis of variance, with the between-subject factor group (2 levels), and the within-subjects factors scene categorization (2 levels) and motor selection (2 levels).

Results. We found that both scene categorization and motor selection demands had overall effects on performance, and that this effect was strongest in the patient group. Even in the more demanding visual condition, we found a significant main effect of motor selection and a significant interaction with group. Since these results were in line with our expectation that both factors of the dual task would equally influence performance, and since consequently performance dropped parametrically from the easiest condition (low motor demand, low visual demand) to the hardest condition

(high motor and visual demands), we concluded that our task indeed served the generally purpose of increasing demand on the central executive, irrespective of the exact source of the demand. For simplicity, in the following and in the main text, we will treat task difficulty as a single factor with four levels (as outlined above).

More specifically, for accuracy, we found main effects for all three factors (group: $F_{1,30}$=25.45, p=0.00002, motor selection: $F_{1,30}$=11.35, p=0.002, scene categorization: $F_{1,30}$=36.18, p=0.000001), and interactions between group and both motor selection ($F_{1,30}$=6.32, p=0.018) and scene categorization ($F_{1,30}$=28.73, p=0.000008). When limiting our analysis to scene categorization trials only (i.e. by omitting the conditions with scrambled scenes), we still found main effects of group and motor selection (group: $F_{1,30}$=29.063, p=0.000008, motor selection: $F_{1,30}$=15.27, p=0.00049) and a significant interaction between group and motor selection ($F_{1,30}$=7.11, p=0.012). This interaction indicates that motor selection demands differentially affected patients even when scene categorization demands were high.

For reaction time, we found main effects for all three factors (group: $F_{1,30}$=16.18, p=0.00036, motor selection: $F_{1,30}$=99.59, $p<10^{-6}$, scene categorization: $F_{1,30}$=113.36, $p<10^{-6}$), and interactions between group and both motor selection ($F_{1,30}$=4.54, p=0.041) and scene categorization ($F_{1,30}$=14.59, p=0.001). When limiting our analysis to scene categorization trials only (i.e. by omitting the conditions with scrambled scenes), we still found main effects of group and motor selection (group: $F_{1,30}$=18.20, p=0.00018, motor selection: $F_{1,30}$=53.9, $p<10^{-7}$), but no significant interaction between group and motor selection ($F_{1,30}$=1.78, p=0.192).

Structural MRI: data acquisition and voxel-based morphometry (VBM)

Data acquisition. To investigate the degree of brain atrophy and its potential influence on functional connectivity in patients with pAD, participants were assessed by structural MRI. MRI was performed on a 3 T whole body MR scanner (Achieva, Philips, Netherlands) using an 8-channel phased-array head coil. T1-weighted anatomical data were obtained from each participant by using a magnetization-prepared rapid acquisition gradient echo sequence (TE = 4 ms, TR = 9 ms, TI = 100 ms, flip angle = 5°, FoV = 240 x 240 mm^2, matrix = 240 x 240, 170 slices, voxel size = 1 x 1 x1 mm^3).

VBM. To analyze structural imaging data, we used voxel-based morphometry (VBM) applying the VBM-toolbox (http://dbm.neuro.uni-jena.de/) implemented in SPM8 using default parameters. Images were bias-corrected, tissue classified, and linearly (i.e., 12-parameter affine registration) and non-linearly (i.e., warping regularization) registered. Subsequently, gray matter (GM) and white matter (WM) segments were modulated by multiplication with the non-linear components derived from the normalization matrix in order to preserve actual GM and WM values locally. Finally, images were smoothed with a Gaussian kernel of 8 mm full-width at half maximum (FWHM). Voxel-wise GM differences between patients and controls were examined using two-sample t-tests. In order to avoid possible edge effects between different tissue types, absolute threshold masking was applied (i.e., all voxels with GM of less than 0.1 were excluded). GM group comparisons were based on a threshold of $p<0.05$ FWE cluster-corrected. Finally, to control for the influence of brain atrophy on functional connectivity, gray matter values were extracted from those networks showing group differences in connectivity that were spatially consistent across rest

and task condition. These gray matter values (averaged for the respective networks) were entered as a covariate in the functional connectivity group comparison.

PIB-PET analysis.

Ddata acquisition and analysis. Both PET-imaging with N-methyl-^{11}C-2-(4-methylaminophenyl)-6-hydroxybenzothiazole (i.e. PiB tracer) and data analysis followed standard protocols as described in a previous study (Mosconi et al., 2008). All participants were injected with 370 MBq ^{11}C-PIB at rest before entering the scanner thirty minutes later. 40 minutes post-injection, three 10-minute frames of data acquisition were started and later summed into a single frame (40-70 minutes). Acquisition was performed using a Siemens ECAT HR+ PET scanner (CTI, Knoxville, Tenn., USA) in 3D mode and a transmission scan was carried out subsequently to allow for later attenuation correction.

Data analysis. The first step of imaging data analysis consisted of image reconstruction, correction of dead time, scatter and attenuation. Statistical parametric mapping software (SPM 5, Wellcome Department of Cognitive Neurology, London, UK) was used for image realignment, transformation into standard stereotactic Montreal Neurological Institute (MNI) space (MNI PET template), smoothing and statistical analysis (Mosconi et al., 2008). For More specifically, for spatial transformation of PiB-data, standardized uptake value (SUV) images (40-70 min p.i.) were co-registered to each individual's volumetric MRI and then automatically spatially normalized to the MNI-template in SPM5 using warping parameters derived from normalizing the structural scan using DARTEL the 'Unified Segmentation' tool and warping parameters derived from previous individual MRI-normalization (Mosconi et al., 2008). For each subject, all voxel values were normalized to the cerebellar vermis, and images were smoothed (Gaussian kernel of 10 mm x 10 mm x 10 mm). Whole brain voxel-wise group comparisons (two-sample t-test) were

performed with a threshold of $p<0.001$ uncorrected and minimum cluster extent $k=100$.

Supplementary Figures:

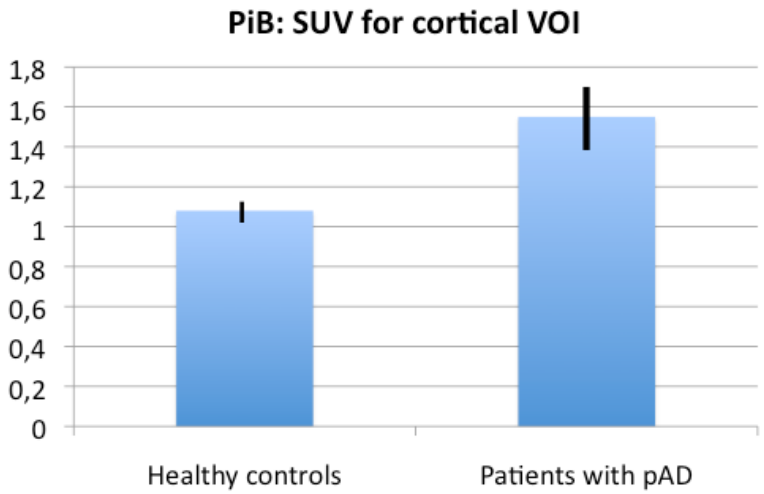

Figure S1. Mean standardized uptake value (SUV) for large cortical volume of interest (VOI). Mean PiB-uptake scores in patients and healthy participants within pre-established large cortical volume of interest (VOI) including lateral prefrontal, parietal, and temporal areas and the retrosplenial cortex (Hedden et. al, 2009, Drzega et al., 2011). Cut-off for 'high' or 'low' neocortical standardized uptake value (SUV) ratios was 1.15 (Hedden et al, 2009, Drzezga et al., 2011). Persons with high PiB binding (i.e. standardized uptake ratio ≥ 1.15) were classified as PiB-positive and those with standardized uptake ratio smaller than 1.15 were classified as PiB-negative. All patients were PiB-positive, all controls PiB-negative.

Figure S2. Stimulus material of fMRI paradigm. Sample images for grayscale picture of country road (left), city street (middle) and scrambled scene (right).

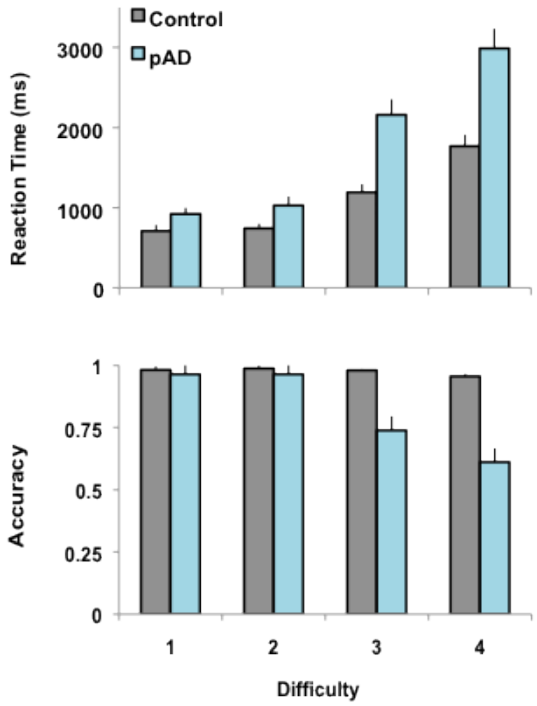

Figure S3. Behavioral results of the attention-demanding task with 4 difficulty levels.

Overall, reaction times (RT, top plot) increased and accuracy (ACCR, bottom plot) decreased with increasing difficulty (1: scrambled images, one response hand; 2: scrambled images, two response hands; 3: scene categorization, one response hand; 4: scene categorization, two response hands; ACCR $F(3,90)=30.7$, $p<0.001$; RT $F(3,90)=93.7$, $p<0.001$). Prodromal AD (pAD) patients performed worse than controls (ACCR $F(1,30)=25.4$, $p<0.001$; RT $F(1,30)=16.2$, $p<0.001$), mainly in the most difficult condition (independent t-tests, ACCR $t(30)=5.51$, $p < 0.001$, RT $t(30)=-3.99$, $p < 0.001$), leading to a significant interaction between group and condition (ACCR $F(3,90)=23.3$, $p<0.001$; RT $F(3,90)=10.7$, $p<0.001$).

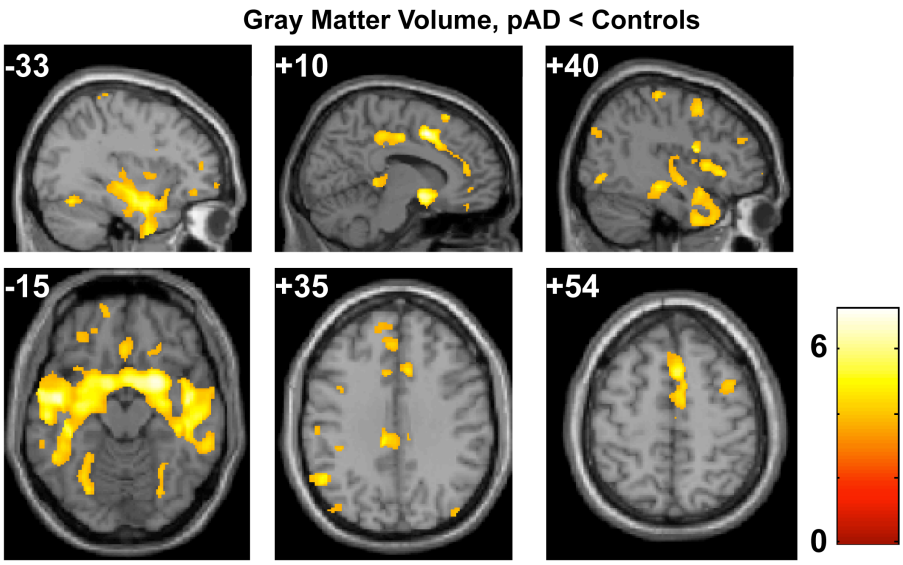

Figure S4. Voxel-based morphometry (VBM) of structural MRI derived from patients with prodromal AD and healthy elderly. Plotted is a map of two-sample t-test contrasting pAD and control groups. The significance level is $p<0.001$ uncorrected for multiple comparisons, demonstrating that even for rather liberal threshold, the majority of group differences is restricted to the medial and lateral anterior temporal lobes, extending into the amygdala, ventral striatum, and anterior cingulate. Notably, only sparse GM differences are in the lateral parietal and prefrontal cortex, as well as the posterior default mode regions overlapping with DMN and attention networks (also indicated in table S2).

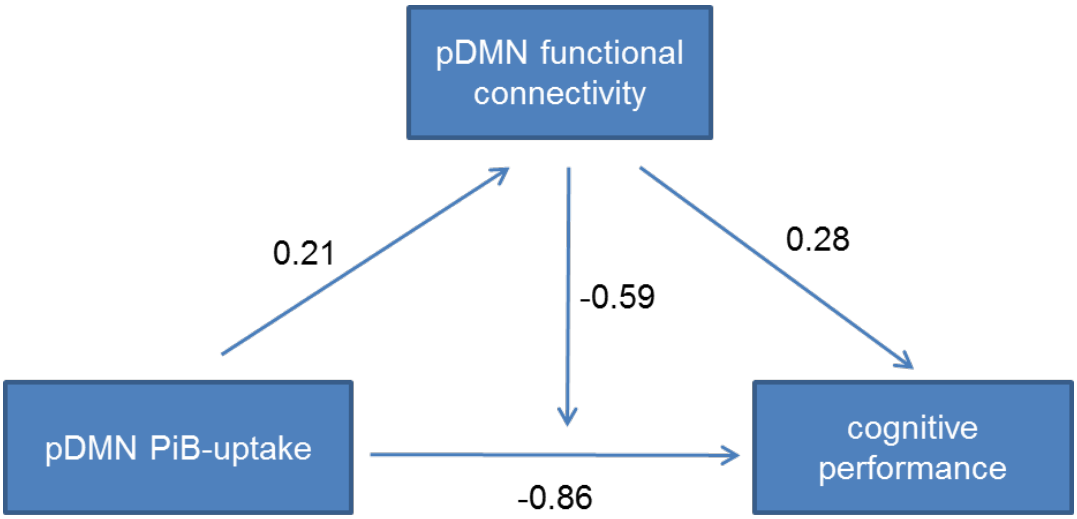

Figure S5. Structural equation modeling (SEM) results. Structural equation modeling shows a moderating effect of pDMN functional connectivity on the association between pDMN PiB-uptake and cognitive (i.e., ACCR4-ACCR1) performance (β=-0.59, $p<0.001$).

Supplementary Tables

Table S1: Center coordinates and spatial extent of pDMN and rATN showing an overlap between rest and task group differences.

Overlap region	Center coordinates	Cluster size	Area
pDMN	x=4, y=-70, z=34	k=15	Precuneus
rATN	x=40, y=-64, z=48	k=3	Inf. Parietal lobule

Overlap results are based on single two-sample t-tests, p<0.05 FWE cluster-corrected, for each network and condition.

Table S2: Gray Matter Differences between Patients and Controls measured by VBM

Anatomical region	L/R	cluster size	Z-score	T-score	p-value	x (MNI)	y	Z
Controls > Patients, two-sample-t-test								
cingulate gyrus superior frontal gyrus medial frontal gyrus	L/R	13458	5.71	7.25	<0.001	10	8	46
Sup/med temporal gyrus parahippocampal gyrus medial temporal lobe	L/R	56041	5.55	6.95	<0.001	56	-24	-5
postcentral gyrus	R	878	4.52	5.24	<0.001	45	-25	63
superior frontal gyrus middle frontal gyrus	R	799	4.22	4.81	<0.001	30	58	1
superior orbitofrontal gyrus	R	907	3.94	4.41	<0.001	18	34	-26

Table shows all clusters with p<0.05, FWE cluster-corrected.

Table S3: ICN peak activity and group differences during rest and task.

Posterior Default Mode Network						
Anatomical region	L/R	cluster	Z-score	T-score	p-value	MNI (x;y;z)
REST						
Controls, one-sample-t-test						
Precuneus	L	6195	>8	39.71	<0.001	-6;-66;28
Precuneus	R		>8	34.98	<0.001	8;-62;32
Posterior Cingulate Cortex	R		6.58	16.56	<0.001	2;-32;36
Posterior Cingulate Cortex	L		6.85	18.86	<0.001	-4;-44;32
Inferior Parietal Lobule	R		7.61	27.78	<0.001	40;-62;34
Inferior Parietal Lobule	L	521	5.20	8.99	0.018	-42;-60;28
Anterior Medial Prefrontal Cortex	R	4	5.14	8.78	0.025	6;48;2
Patients, one-sample-t-test						
Precuneus	L	11051	>8	36.86	<0.001	-4;-68;32
Precuneus	R		>8	29.73	<0.001	6;-66;34
Posterior Cingulate Cortex	R		>8	26.28	<0.001	4;-44;24
Posterior Cingulate Cortex	L		>8	25.72	<0.001	-2;-56;30
Inferior Parietal Lobule	L		>8	19.82	<0.001	-40;-62;38
Inferior Parietal Lobule	R		7.01	13.40	<0.001	48;-60;28
Anterior Medial Prefrontal Cortex	L	10	5.19	7.28	0.015	-6;48;4
Controls>Patients, two-sample-t-test						
Precuneus	R	24	4.14	4.69	0.022	8;-66;32
TASK						
Controls, one-sample-t-test						
Precuneus	L	4692	6.42	16.58	<0.001	-14;-64;20
Precuneus	R		7.68	32.32	<0.001	6;-58;32
Posterior Cingulate Cortex	R		>8	36.60	<0.001	4;-38;26
Posterior Cingulate Cortex	L		>8	36.92	<0.001	-2;-52;32
Inferior Parietal Lobule	R	335	6.63	18.36	<0.001	48;-62;26
Inferior Parietal Lobule	L	157	5.74	11.98	0.001	-38;-70;42
Anterior Medial Prefrontal Cortex	L	46	6.11	14.28	<0.001	-2;54;2
Patients, one-sample-t-test						
Precuneus	L	4993	6.66	16.03	<0.001	-6;-68;34
Precuneus	R		7.75	27.06	<0.001	12;-62;26
Posterior Cingulate Cortex	R		>8	28.81	<0.001	6;-54;28
Posterior Cingulate	L		6.82	17.27	<0.001	-2;-42;38

Cortex						
Inferior Parietal Lobule	R	498	5.63	10.31	0.002	42;-70;34
Inferior Parietal Lobule	L	217	5.84	11.25	<0.001	-40;-68;38
Anterior Medial Prefrontal Cortex	R	35	5.85	11.31	<0.001	8;50;4
Patients>Controls, two-sample-t-test						
Precuneus	R	36	4.07	4.75	0.005	18;-72;32

Anterior Default Mode Network						
Anatomical region	L/R	cluster	Z-score	T-score	p-value	MNI (x;y;z)
REST						
Controls, one-sample-t-test						
Superior Medial Gyrus	L	5395	7.25	22.99	<0.001	-6;52;36
Superior Medial Gyrus	R		6.71	17.65	<0.001	6;52;30
Pregenual Anterior Cingulate Cortex	L		7.07	21.02	<0.001	-4;50;12
Pregenual Anterior Cingulate Cortex	R		5.84	11.86	<0.001	10;40;28
Angular Gyrus	L	309	6.75	17.97	<0.001	-54;-60;30
Posterior Cingualte Cortex	L/R	182	5.93	12.30	<0.001	+/- 2;-54;24
Patients, one-sample-t-test						
Superior Medial Gyrus	R	7771	>8	27.75	<0.001	8;56;20
Superior Medial Gyrus	L		>8	22.18	<0.001	-6;44;36
Pregenual Anterior Cingulate Cortex	L/R		7.42	15.48	<0.001	0;42;12
Posterior Cingualte Cortex	L	861	6.94	13.09	<0.001	-2;-52;32
Angular Gyrus	L	395	6.17	10.06	<0.001	-52;-58;28
TASK						
Controls, one-sample-t-test						
Superior Medial Gyrus	L/R	5176	7.14	23.91	<0.001	0;62;10
Pregenual Anterior Cingulate Cortex	R		6.79	19.91	<0.001	2;42;10
Pregenual Anterior Cingulate Cortex	L		6.25	15.21	<0.001	-6;38;24
Angular Gyrus	L	53	5.68	11.66	0.001	-50;-60;30
Posterior Cingualte Cortex	L/R	2	5.06	8.83	0.039	0;-54;30
Patients, one-sample-t-test						
Sup. Medial Gyrus	R	6364	7.62	25.32	<0.001	4;64;24
Superior Medial Gyrus	L		7.40	22.66	<0.001	-4;54;24
Pregenual Anterior Cingulate Cortex	L/R		7.32	21.86	<0.001	0;40;20
Precuneus	L	67	5.45	9.58	0.005	-2;-62;24

Right Attention Network						
Anatomical region	L/R	cluster	Z-score	T-score	p-value	MNI (x;y;z)
REST						
Controls, one-sample-t-test						
Inferior Parietal Lobule	R	2234	>8	40.74	<0.001	44;-58;46
Middle Frontal Gyrus	R	2003	7.50	26.18	<0.001	44;20;48
Superior Frontal Gyrus	R	930	7.04	20.71	<0.001	22;60;6
Medial Frontal Gyrus	R	345	5.70	11.15	0.001	10;44;40
Cerebellum	L	52	5.47	10.09	0.004	-10;-80;-30
Patients, one-sample-t-test						
Middle Frontal Gyrus	R	7633	7.63	16.74	<0.001	36;16;48
Superior Frontal Gyrus	R		6.48	11.17	<0.001	16;34;60
Medial Frontal Gyrus	R		6.93	13.02	<0.001	10;34;38
Inferior Parietal Lobule	R	2899	>8	21.04	<0.001	52;-56;50
Cerebellum	L	1068	7.05	13.57	<0.001	-34;-72;-44
Controls>Patients, two-sample-t-test						
Inferior Parietal Lobule	R	19	4.15	4.70	0.044	50;-58;50
TASK						
Controls, one-sample-t-test						
Inferior Parietal Lobule	R	2022	>8	36.24	<0.001	50;-56;44
Inferior Parietal Lobule	L	321	6.64	18.52	<0.001	-40;-54;36
Middle Frontal Gyrus	R	250	6.31	15.70	<0.001	38;16;56
Medial Frontal Gyrus	R	45	5.62	11.33	0.002	6;42;36
Superior Frontal Gyrus	R	22	5.98	13.39	<0.001	24;28;58
Cerebellum	L	13	5.48	10.66	0.004	-26;-72;-32
Patients, one-sample-t-test						
Inferior Parietal Lobule	R	2718	7.71	26.49	<0.001	56;-60;32
Inferior Parietal Lobule	L	487	6.47	14.72	<0.001	-42;-58;38
Middle Frontal Gyrus	R	93	5.54	9.91	0.003	34;14;58
Medial Frontal Gyrus	R	32	5.75	10.85	<0.001	8;34;46
Superior Frontal Gyrus	R	7	5.27	8.91	0.012	24;24;56
Cerebellum	L	2	5.08	8.23	0.035	-28;-68;-28
Patients>Controls, two-sample-t-test						
Inferior Parietal Lobule/Middle Occipital Gyrus	R	33	4.72	5.81	0.006	36;-80;32

Left Attention Network						
Anatomical region	L/R	cluster	Z-score	T-score	p-value	MNI (x;y;z)
REST						
Controls, one-sample-t-test						

Inferior Parietal Lobule (Angular Gyrus)	L	1715	7.25	22.87	<0.001	-52;-56;42
Middle Frontal Gyrus	L	575	7.14	21.74	<0.001	-38;28;46
Superior Frontal Gyrus	L		5.95	12.43	<0.001	-24;16;66
Inferior Frontal Gyrus	L	236	5.81	11.66	<0.001	-48;36;-16
Inferior Parietal Lobule (Angular Gyrus)	R	44	5.43	9.90	<0.001	60;-44;38
Patients, one-sample-t-test						
Inferior Parietal Lobule (Angular Gyrus)	L	2864	>8	22.54	<0.001	-46;-62;52
Superior and Middle Frontal Gyrus	L	1755	7.45	15.68	<0.001	-42;20;48
Inferior Frontal Gyrus	L	579	6.83	12.58	<0.001	-40;46;-16
Inferior Parietal Lobule (Angular Gyrus)	R	903	>8	19.62	<0.001	56;-58;40
Cerebellum	R	960	6.64	11.80	<0.001	38;-64;-40
TASK						
Controls, one-sample-t-test						
Inferior Parietal Lobule (Angular Gyrus)	L	2160	7.62	31.18	<0.001	-54;-52;34
Middle Frontal Gyrus	L	553	7.27	25.70	<0.001	-40;18;42
Cerebellum	R	111	6.07	14.02	<0.001	40;-66;-46
Patients, one-sample-t-test						
Inferior Parietal Lobule (Angular Gyrus)	L	2843	>8	36.53	<0.001	-48;-58;44
Middle Frontal Gyrus	L	534	7.15	20.13	<0.001	-38;16;52
Cerebellum	R	180	5.64	10.33	0.002	24;-78;-32

Dorsal Attention Network						
Anatomical region	L/R	cluster	Z-score	T-score	p-value	MNI (x;y;z)
REST						
Controls, one-sample-t-test						
Superior and Inferior Parietal Lobule	L	5849	7.64	28.15	<0.001	-30;-56;48
Precuneus	L		7.28	23.34	<0.001	-12;-72;46
Precuneus	R		7.45	25.45	<0.001	12;-72;50
Superior and Inferior Parietal Lobule	R		7.24	22.93	<0.001	22;-72;50
Patients, one-sample-t-test						
Superior and Inferior Parietal Lobule	R	9743	>8	27.08	<0.001	24;-70;52
Precuneus	R		>8	22.97	<0.001	8;-64;50
Superior and Inferior Parietal Lobule	L		>8	22.92	<0.001	-26;-64;54
Precuneus	L		>8	19.88	<0.001	-4;-52;62
TASK						
Controls, one-sample-t-test						
Angular Gyrus;Superior and Inferior Parietal	R	5925	7.27	25.71	<0.001	32;-54;44

Lobule						
Precuneus	R		7.03	22.54	<0.001	6;-56;56
Precuneus	L		7.20	24.67	<0.001	-12;-70;48
Superior and Inferior Parietal Lobule	L		7.11	23.57	<0.001	-18;-64;50
Patients, one-sample-t-test						
Angular Gyrus;Superior and Inferior Parietal Lobule	R	6550	>8	32;57	<0.001	32;-60;44
Precuneus	R		7.38	22.44	<0.001	10;-54;54
Superior and Inferior Parietal Lobule	L		7.82	28.31	<0.001	-18;-58;54
Precuneus	L		7.43	23.03	<0.001	-4;-54;50
Patients>Controls, two-sample-t-test						
Angular Gyrus	R	20	4.33	5.15	0.014	34;-62;46

Salience Network						
Anatomical region	L/R	cluster	Z-score	T-score	p-value	MNI (x;y;z)
REST						
Controls, one-sample-t-test						
Middle and Superior Frontal Gyrus	L	2094	7.23	22.81	<0.001	-36;36;32
Anterior Cingulate Cortex	R		6.13	13.48	<0.001	8;32;20
Middle and Superior Frontal Gyrus	R	1045	6.50	16.00	<0.001	32;40;28
Insula Lobe	L	239	6.73	17.77	<0.001	-32;16;10
Superior Orbital Gyrus	R	88	5.69	11.07	0.001	24;50;0
Insula Lobe	R	53	5.82	11.72	0.001	32;18;-8
Patients, one-sample-t-test						
Middle and Superior Frontal Gyrus	R	6851	7.84	18.24	<0.001	30;48;22
Middle and Superior Frontal Gyrus	L		7.77	17.69	<0.001	-26;48;14
Anterior Cingulate Cortex	R		6.47	11.14	<0.001	6;32;32
Insula Lobe	L		6.84	12.63	<0.001	-32;12;6
Insula Lobe	R	329	5.76	8.77	0.001	36;24;-2
TASK						
Controls, one-sample-t-test						
Middle and Inferior Frontal Gyrus	L	1225	7.16	24.24	<0.001	-50;20;28
Middle and Inferior Frontal Gyrus	R	559	6.18	14.72	<0.001	44;14;28
Inferior Parietal Lobule	L	620	7.09	23.26	<0.001	-32;-64;42
Inferior Parietal Lobule	R	158	6.48	17.08	<0.001	36;-64;36
Patients, one-sample-t-test						
Middle and Inferior Frontal Gyrus	R	1422	7.25	21.15	<0.001	52;24;30

Middle and Inferior Frontal Gyrus	L	1517	6.69	16.31	<0.001	-44;28;18
Inferior Parietal Lobule	L	675	6.86	17.56	<0.001	-28;-56;38
Inferior Parietal Lobule	R	107	6.12	12.64	<0.001	32;-70;36

Primary Auditory Network						
Anatomical region	L/R	cluster	Z-score	T-score	p-value	MNI (x;y;z)
REST						
Controls, one-sample-t-test						
Insula/Superior Temporal Gyrus	L	1894	7.38	24.52	<0.001	-42;-20;12
Insula/Superior Temporal Gyrus	R	1462	7.11	21.41	<0.001	44;-20;8
Anterior Cingulate Cortex	L/R	294	5.93	12.31	<0.001	0;20;16
Patients, one-sample-t-test						
Insula/Superior Temporal Gyrus	L	3791	>8	19.87	<0.001	-54;-30;8
Insula/Superior Temporal Gyrus	R	3067	>8	20.50	<0.001	60;-16;12
Anterior Cingulate Cortex	L/R	1370	7.09	14.62	<0.001	0;24;30
TASK						
Controls, one-sample-t-test						
Insula/Superior Temporal Gyrus	L	2214	7.45	28.33	<0.001	-62;-14;6
Insula/Superior Temporal Gyrus	R	1054	7.16	24.21	<0.001	56;-18;6
Patients, one-sample-t-test						
Insula/Superior Temporal Gyrus	L	3156	>8	33.40	<0.001	-60;-24;16
Insula/Superior Temporal Gyrus	R	1216	7.05	19.24	<0.001	64;-18;12
Anterior Cingulate Cortex	L/R	37	5.38	9.29	<0.001	0;28;26

One- and two-sample-t-tests are thresholded at $p<0.05$ FWE cluster-corrected.

Table S4: Spatial correlation of ICNs during rest and task

ICN	Correlation coefficient for rest and task ICN
Posterior Default Mode Network	0.823
Anterior Default Mode Network	0.872
Right Attention Network	0.762
Left Attention Network	0.705
Dorsal Attention Network	0.794
Primary Auditory Network	0.752
Salience Network	0.522

In order to match corresponding ICNs in resting state and task condition, we created templates from identified resting state networks in a whole group approach ($p<0,05$, FWE cluster-corrected). These masks have been spatially correlated with the 59 components of the task ICA-analysis with the gift-toolbox.

Table S5: Correlation analyses of consistently disrupted ICN-regions with dual task accuracy, CERAD total score, and local PiB in patients

Anatomical region	L/R	cluster	Correlation	Max T-score	p-value	MNI (x;y;z)
Task accuracy						
pDMN						
Cuneus	L/R	208	Positive	4.77	<0.001	0;-82;34
rATN						
Superior Parietal Lobule	R	62	Positive	2.47	0.013	44;-56;54
CERAD total						
pDMN						
Cuneus/Precuneus	L	409	Positive	4.38	<0.001	-12;-72;28
Cuneus	R	51	Positive	2.34	0.015	22;-70;24
rATN						
Superior Parietal Lobule/ Angular Gyrus	R	429	Positive	5.25	<0.001	26;-74;54
Local PiB						
pDMN						
Cuneus/Precuneus	L	50	Negative	2.52	0.010	-8;-80;26
rATN						
Inferior Parietal Lobule	R	46	Negative	2.57	0.009	50;-60;50

Patients' scores for dual task accuracy, CERAD-total, and local PiB-uptake were treated as continuous variables and regressed per voxel against pDMN/rATN functional connectivity maps, resulting in corresponding SPMs ($p<0.05$ uncorrected and $k=40$).

References

Baron RM, Kenny DA (1986) The moderator-mediator variable distinction in social psychological research: conceptual, strategic, and statistical considerations. *J Pers Soc Psychol 51*(6):1173-1182.

Drzezga, A., Becker, J. A., Van Dijk, K. R. A., Sreenivasan, A., Talukdar, T., Sullivan, C., et al. (2011). Neuronal dysfunction and disconnection of cortical hubs in non-demented subjects with elevated amyloid burden. *Brain*, *134*(6), 1635–1646.

Hedden, T., Van Dijk, K. R. A., Becker, J. A., Mehta, A., Sperling, R. A., Johnson, K. A., & Buckner, R. L. (2009). Disruption of functional connectivity in clinically normal older adults harboring amyloid burden. *Journal of Neuroscience*, *29*(40), 12686–12694.

Koch K., Wagner G., Schachtzabel C., Schultz C.C., Güllmar D., Reichenbach J.R., Sauer H., Schlösser R.G. (2013) Age-dependent visuomotor performance and white matter structure: a DTI study. *Brain Struct Funct 218*(5): 1075-84.

Schlösser RGM, Koch K, Wagner G (2007) Assessing the State Space of the Brain with fMRI: An Integrative View of Current Methods. *Pharmacopsychiatry 40*(Suppl. 1):85-92.